ACS OMEGA

http://pubs.acs.org/journal/acsodf

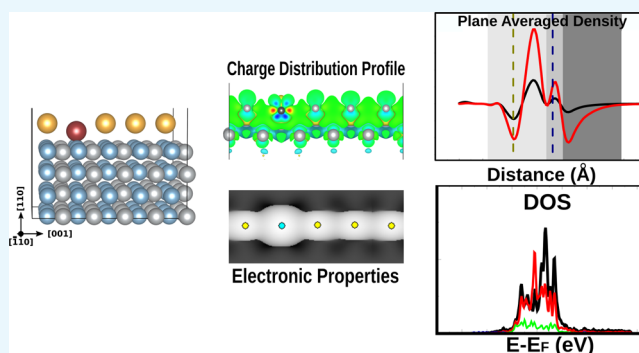# Theoretical Insights into 1D Transition-Metal Nanoalloys Grown on the NiAl(110) Surface

Bruno Fedosse Zornio,[†] Edison Zacarias da Silva,[‡] and Miguel Angel San-Miguel*,[†]

[†]Department of Physical Chemistry, Institute of Chemistry (IQ), University of Campinas (UNICAMP), 13084-862 Campinas, São Paulo, Brazil

[‡]Institute of Physics "Gleb Wataghin" (IFGW), University of Campinas (UNICAMP), 13083-859 Campinas, São Paulo, Brazil

S *Supporting Information*

ABSTRACT: Metallic nanoalloys are essential because of the synergistic effects rather than the merely additive effects of the metal components. Nanoscience is currently able to produce one-atom-thick linear atomic chains (LACs), and the NiAl(110) surface is a well-tested template used to build them. We report the first study based on ab initio density functional theory methods of one-dimensional transition-metal (TM) nanoalloys (i.e., LACs) grown on the NiAl(110) surface. This is a comprehensive and detailed computational study of the effect of alloying groups 10 and 11 metals (Pd, Pt, Cu, Ag, and Au) in LACs supported on the NiAl(110) surfaces to elucidate the structural, energetic, and electronic properties. From the TM series studied here, Pt appears to be an energy-stabilization species; meanwhile, Ag has a contrasting behavior. The work function changes because the alloying in LACs was satisfactorily explained from the explicit surface dipole moment calculations using an ab initio calculation-based approach, which captured the electron density redistribution upon building the LAC.

INTRODUCTION

Technological evolution led to the development of powerful and delicate microscopic techniques, in such a way that in the early 1990s, it became possible to image at an atomic scale using transmission electron microscopes. Furthermore, the use of new probes such as scanning tunneling microscopes (STMs) and atomic force microscopes allowed atoms to be controlled and manipulated at the subnanometric scale.[1,2]

These microscopic techniques allowed the scientific community to build ultrathin one-dimensional (1D) wires. Specifically, one-atom-width wires [or linear atomic chains (LACs)] exhibit unique mechanical[3,4] and electrical transport properties,[5,6] displaying enormous potential as electronic components in nanodevices.

Certainly, a major challenge in nanotechnology is the miniaturization, up to the atomic scale, of electronic circuits,[7] and these techniques have demonstrated that the manipulation of single atoms to build desired nanostructures is today a reality.

However, building LACs requires very delicate experimental apparatus, and producing such devices on an industrial scale is still far from reality. Computational models and atomistic simulations become an essential approach to gain insights into different physical−chemical processes occurring in materials science, which can sometimes be too complex. The low dimensionality of LACs attracted the attention of some research groups, and several joint experimental and computational studies have been reported.

Thus, electron-conductance measurements were interpreted from theoretical calculations on freestanding[8] C LACs, also on supported Cu LACs on the Cu(111) surface,[9] and single-supported[10] or double-supported[11] nanowires.

In another study, experimental measurements for free-standing Au LACs found unusually longer Au−Au bond distances;[12] this fact can be generally attributed to the presence of atomic impurities. A complementary study using ab initio simulations showed a chemical process in which an O_2 molecule can adsorb on an Au LAC, aiding the oxidation of the CO molecule to CO_2 and leaving an oxygen impurity in the Au LAC.[13] This observation opened up the use of LACs as selective catalysts.

Searching for new and innovative materials for catalysis is a permanent goal in several branches of chemistry, physics, and engineering. Transition metals (TMs), especially groups 10 and 11, are well-known catalyst components. In the context of nanotechnology, the ability to produce several types of alloys at the nanometric scale (nanoalloys), by mixing noble/non-noble metals to obtain a material with innovative properties and with a lower cost is a very interesting pursuit. Thus, nanoalloys

based on Pd/Pt,[14] Pt/Ag,[15] or Cu/Au[16,17] have successfully been used for catalytic purposes.

The idea of mixing metals at the nanometric scale to produce nanoalloys is usually associated with the improvement of desired properties synergistically, and the interest in such systems has been increasing in the last few years.[18]

The use of computational methods to understand the physical−chemical properties of nanoalloys appears to be an attractive approach to provide a way to design novel nanoalloys with desired properties. However, aspects concomitant to the 3D dimensionality such as a high number of configurations for each composition, system size, and morphology restrict the number of theoretical studies to a limited number of cases.[19−21] For these reasons, the low dimensionality of LACs allows to carry out systematic studies to better understand the dominant effects in nanoalloys.

In the context of catalysis, 1D nanoalloys might have a potential application as selective adsorption traps for molecules. Specifically, alloying LACs appears to be an adequate tool to tune the adsorption capability of the pristine LACs for specific molecules. Therefore, the combination of low dimensionality[22] and alloying[23,24] can enhance, for example, single-molecule spectroscopic properties, possibly assisting in establishing a reaction mechanism[24] or the use as molecular sensors.[25]

On the basis of the high predictive capability of the density functional theory (DFT) computer modeling of solids and nanostructures, we aim to investigate the structural and electronic properties of low-dimensionality nanoalloys, looking forward to a better rationalization of the combination effects of alloying TMs on supported LACs. Specifically, we are interested in supported groups 10- and 11-alloyed LACs on the NiAl(110) surface.

Regarding the substrate, the unique properties of the NiAl(110) surface make it a notable and well-established substrate to understand the adsorption processes.[26−29] Several reported computer simulation studies focused on atomic adsorption processes,[30−32] molecular adsorption,[33−35] and the impressive ability to build interesting structures on these substrates.[36−38]

Precisely, our work is inspired by the studies led by Nilius et al. in the early 2000s.[39−43] These experiments demonstrated the ability of experimentally building Au and Pd LACs on NiAl(110) and lead us to suggest that alloying might be a realistic approach to create novel systems with desired functionalities;[42] therefore, we aim to study alloyed LACs, hoping to provide new and exciting results to help the understanding of the physical−chemical properties of these systems and motivate new experiments.

In this article, we first describe the computational model used for the simulations and some relevant substrate features. Next, the discussion starts with a structural investigation followed by an energetic stability analysis. The subsequent section tackles the electronic properties, focusing on the nature of the substrate−chain interactions, and complementarily an analysis of the work function and the dipole moment is also presented. Finally, the conclusion section ends presenting the main contributions of this study.

■ COMPUTATIONAL MODEL

The computational model to describe the NiAl(110) surface was based on a previously reported body-centered cubic NiAl bulk calculation.[35] In good agreement with experimental

data,[44] d_0 was estimated to be 2.91 Å, and the lattice parameters for the [001] and [$\bar{1}$10] directions were set as d_0 and $\sqrt{2}d_0$, respectively. The NiAl(110) slab was built from a (3 × 5 × 4) supercell with an ~26 Å vacuum distance to guarantee a negligible interaction between the slab surfaces.

As widely reported, the fourfold Ni−Ni bridge is the most stable adsorption site,[30,31,35,36] and the deposited LAC atoms locate on them. It is also important to note that, as previously shown, because of the distance between the adsorption sites, the only direction possible to form the LACs is [001]; consequently, this is the case studied here.[38,45]

The alloying effect was studied starting from the pristine LAC model[45] with the subsequent substitution of one chain atom by a dopant, another group 10 or 11 atom. Because of the slab size and the periodic boundary conditions, five positions are available on the surface to build the LAC. Thus, in this model, the atomic chain is formed by four main types of atoms and one dopant (i.e., 20% alloying composition). Figure 1 depicts the nanoalloy model used.
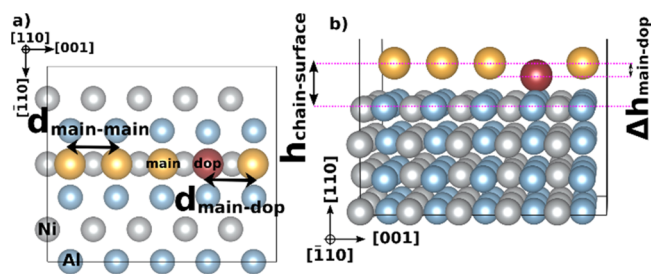

Figure 1. Ni and Al atoms are shown in light gray and blue, respectively. The golden spots represent the main LAC atoms, and the rusty red spot represents the dopant. (a) Top view: Distances between the main atoms in the chain ($d_{\text{main−main}}$) and the distance between the main atom and the dopant in the chain ($d_{\text{main−dop}}$). (b) Side view: The height of the main chain ($h_{\text{chain−surface}}$) and the relative height between the main chain and the dopant ($\Delta h_{\text{main−dop}}$).

■ RESULTS AND DISCUSSION

Chain Structure and Stability. The effect of the dopant on the geometric structure can be visualized in Figure 2. Tables containing the corresponding numerical values can be found in the Supporting Information (Tables S1−S4). The distance between the adatoms in the pristine chains is constant (2.91 Å) for all cases as expected because all adatoms occupy equivalent Ni−Ni bridge adsorption sites, and these positions are constrained to the supercell dimensions, achieving a highly symmetric setting.[36,38,45,46] However, for the doped systems, the atoms in the chain are not equivalent anymore, and some deformation in the chain structure is expected.

These distortions are easily understood from the atomic radii. Figure 2a,b shows the distances between the main atoms, and the main atom and the dopant, respectively. As Pt and Ag have the shortest and largest radii, respectively, in the TM series considered here,[47,48] the Pt−Pt distances are shorter than in the case of the pristine LAC (Figure 2a); meanwhile, the $d_{\text{Pt−dop}}$ distances are longer (Figure 2b), and an opposite effect is found for Ag, in good agreement with other studies on freestanding[49] and supported chains.[48]

A comparison between the height of the main chain and that of the dopant can be visualized in Figure 2c. The main-chain position is set as the reference; therefore, the $\Delta h_{\text{main−dop}}$
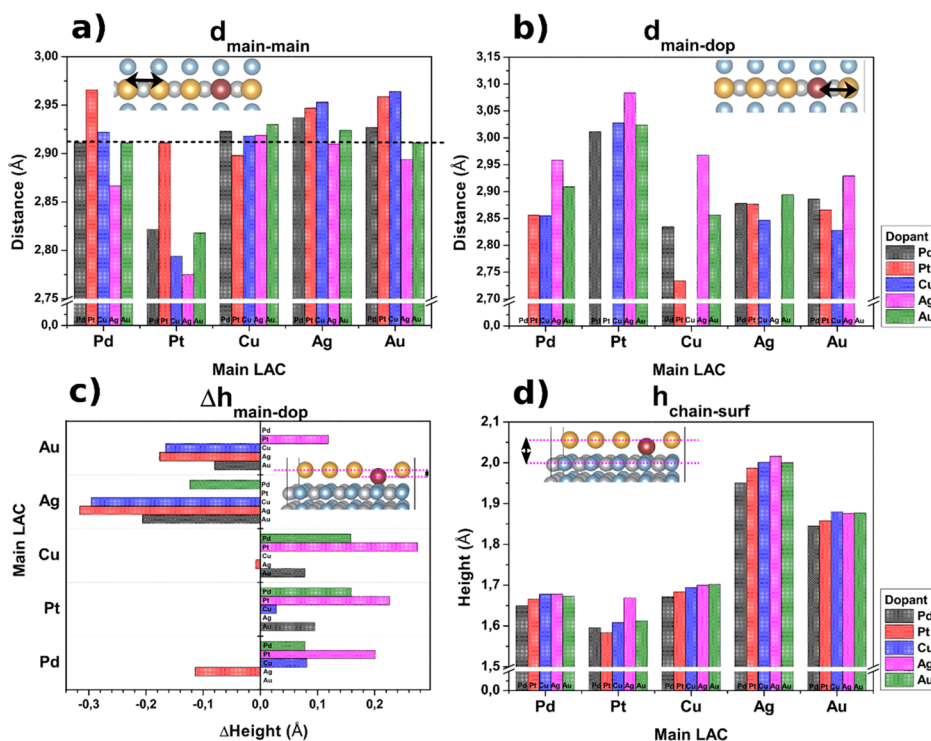
Figure 2. Dopant effects on the chain structure. (a) Distances between the main atoms in the chain, $d_{\text{main-main}}$; the dashed black line indicates d_0, the distance in the pristine system. (b) Distance between the main atom and the dopant, $d_{\text{main-dop}}$. (c) Relative height between the main chain and the dopant, $\Delta h_{\text{main-dop}}$. (d) Distance between the main atom and the dopant in the chain, $h_{\text{chain-surface}}$.
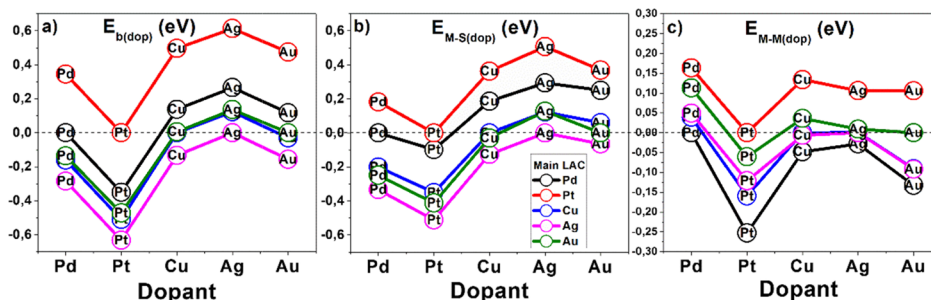

Figure 3. Colored lines indicate the main-chain atoms, and the circles indicate the dopant atom. The pristine system at 0 eV is indicated as a dashed black line. (a) Difference in the binding energy between the mixed and pristine LACs, for all the systems studied, $E_{\text{b(dop)}}$. (b) Difference in the substrate−chain interaction, $E_{\text{M-S(dop)}}$. (c) Difference in the metal−metal interaction along the chain, $E_{\text{M-M(dop)}}$.

positive values indicate that the main-chain atoms are above the dopant position. Thus, the largest atoms (Ag and Au) have negative values, indicating that the dopants are below the main-chain height, in contrast to the smaller atoms (Cu, Pd, and Pt), which generally present positive values.

The system stability was obtained by eq 1, which evaluates the total binding energy for mixed-metal LACs ($E_{\text{b}}^{\text{dop}}$). Equation 1 can be further decomposed into the metal−metal interaction energy ($E_{\text{M-M}}^{\text{dop}}$), given by eq 2, and the chain surface interaction energy ($E_{\text{M-S}}^{\text{dop}}$), given by eq 3.

$$E_{\text{b}}^{\text{dop}} = \frac{E_{\text{tot}} - E_{\text{surf}} - N_{\text{main}}E_{\text{main}} - N_{\text{dop}}E_{\text{dop}}}{N_{\text{main}} + N_{\text{dop}}}$$

$$\equiv E_{\text{M-S}} + E_{\text{M-M}} \tag{1}$$

$$E_{\text{M-S}}^{\text{dop}} = \frac{E_{\text{tot}} - E_{\text{surf}} - E_{\text{chain}}}{N_{\text{main}} + N_{\text{dop}}} \tag{2}$$

$$E_{\text{M-M}}^{\text{dop}} = \frac{E_{\text{chain}} - N_{\text{main}}E_{\text{main}} - N_{\text{dop}}E_{\text{dop}}}{N_{\text{main}} + N_{\text{dop}}} \tag{3}$$

where E_{tot} is the total energy of the computational model; E_{surf} is the bare NiAl slab energy; E_{main}, E_{dop}, and E_{chain} are the energies for the main-chain atom, the dopant, and the LAC system (the chain with the dopant atom) in vacuum, respectively; and N_{main} and N_{dop} are the numbers of atoms in the main chain and the dopants, respectively. For the pristine LAC, $N_{\text{dop}} = 0$ and, in eqs 1−3, the energies become $E_{\text{b}}^{\text{pris}}$, $E_{\text{M-S}}^{\text{pris}}$, and $E_{\text{M-M}}^{\text{pris}}$, respectively.

In the models studied, the absolute value of E_{b} frequently does not provide beneficial information, as has been widely reported.[30,35,36,50] In fact, for the mixed-metal LAC architecture, the absolute values of the stabilization energy are quite meaningful. Therefore, we aim to compare the stability of the mixed-metal LACs to that of the pristine ones. It is important to mention that because of the periodic boundary conditions, an infinite 1D chain is assumed in the particular case of pristine
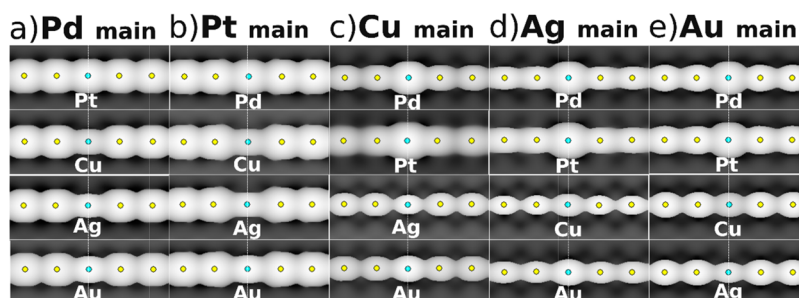
Figure 4. Simulated STM images of the mixed-metal LACs; a theoretical bias voltage of −1.5 V and adjustable height. The main atoms are the yellow dots, and the dopants along the dashed white lines are the blue dots. (a−e) Columns indicate the main-chain atoms.
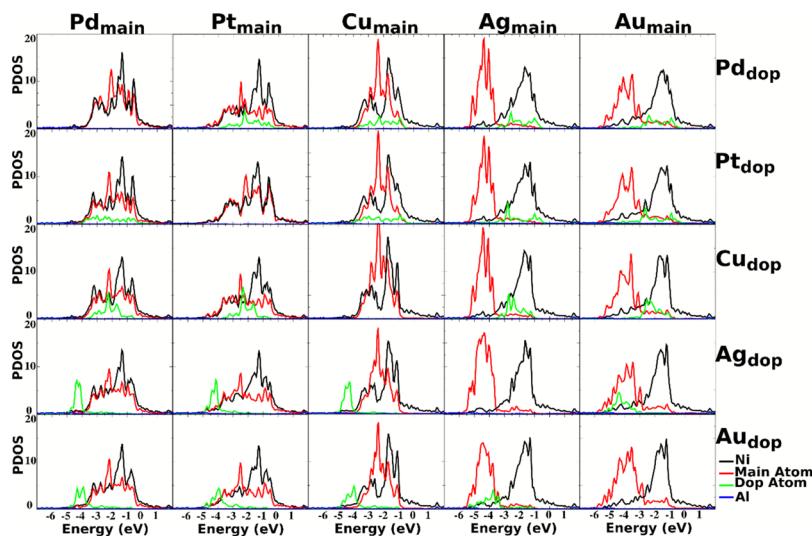

Figure 5. PDOS on the d states for all. Surface Ni and Al are in black and blue lines, respectively. The main LAC atom is in the red lines, and the dopant atom is in the green lines. The pristine LAC PDOS is in the diagonal plots.

LACs; the results are independent of the size of the LAC. However, for the mixed-metal LAC, there is a 20% dopant composition; thus, if different compositions are considered, in other words, different computational models are used, the absolute values of E_b^{dop} might change, but the trends and qualitative results should still be the same.

Figure 3a−c exhibits the E_b, E_{M-S}, and E_{M-M}, respectively (the "dop" subscript indicates that the value in the axis is the difference between the mixed-metal LAC model and the pristine one, e.g., $E_{b(dop)} = E_b^{dop} - E_b^{pris}$). Thus, when the dopant coincides with the main atom (pristine LAC), the energy difference must be null.

Considering Figure 3a (which shows the difference in the total stabilization energy, $E_{b(dop)}$) for group 10, all Pt main LACs (shown in red), regardless of the chemical nature of the dopant, exhibit positive $E_{b(dop)}$ values. This means that all dopants destabilize the pristine Pt LAC. Furthermore, when the dopant is Pt (the cases shown by the circles labeled with Pt), $E_{b(dop)}$ values are significantly negative, pointing out that the system is more stable than the former pristine LAC. In fact, the energy contributions regarding the chain stability ($E_{M-M(dop)}$, Figure 3b) and the substrate chain stability ($E_{M-S(dop)}$, Figure 3c) are also decreased. These results indicate that Pt acts, in all cases, as a stabilization agent for the LAC system. Meanwhile, Pd LACs (black line) also decrease the total stabilization energy ($E_{b(dop)}$) and the chain−substrate stabilization energy ($E_{M-S(dop)}$) for most of the

dopants but Pt. In contrast, the metal−metal stabilization energy ($E_{M-M(dop)}$) is increased.

With respect to group 11 metals, Au- and Cu-based LACs show very similar behaviors with respect to $E_{b(dop)}$. In addition, it is observed that the presence of Ag leads to contrasting behaviors when compared with the other metals. For mixed-metal Ag-based LACs, the dopant acts by decreasing the stabilization energy of the resulting LAC (magenta line in Figure 3a). On the other hand, for Ag as a dopant, higher $E_{b(dop)}$ values are attained. Similar effects are observed for $E_{M-S(dop)}$ and $E_{M-M(dop)}$ energies. Thus, Ag can be considered as a destabilization agent for the system.

Both the chain structural parameters and the system stabilization effects described in this section lead us to partially conclude that the presence of both Pt or/and Ag in the LACs provides a singular behavior.

Electronic Properties. Simulated STM images of the mixed-metal LACs is a very fascinating and meaningful way to start the discussion concerning the electronic properties of the LACs. Figure 4 shows the results of the simulated STM images. In the simulated STM images, the intensity profile contrast between the main atom and the dopant provides an understanding of the surface interatomic interactions along the chain; for example, the systems with a homogeneous intensity profile along the chain have a higher electronic compatibility between the main atoms and the dopant. On the other hand, the more heterogeneous the intensity profile, the lower the
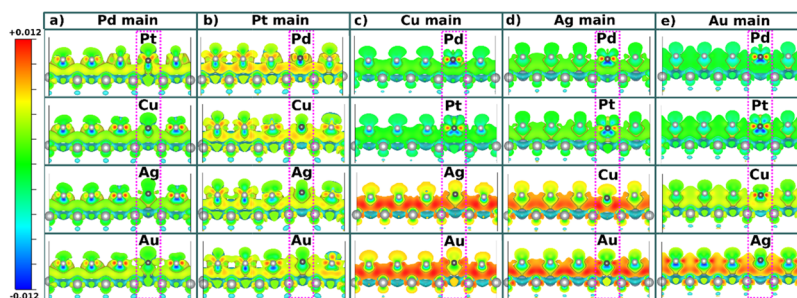
Figure 6. Electron density difference isosurfaces (0.012 e/bohr^3) along the [001] direction (inside cut view). The accumulation or depletion of the electronic charge is indicated using a pallet from red (positive charge) to blue (negative charge). (a,b) Group 10 main LACs and (c−e) group 11 main LACs.

electronic states' coupling between the main atoms and the dopant.

In that sense, a careful analysis of Figure 4 indicates that for systems based on mixing metals from the same group (i.e., mixing Ag/Au/Cu or Pd/Pt), the pictures display homogeneous intensity profiles along the chain. Otherwise, the systems based on mixing atoms from different groups show heterogeneous intensity profiles.

Another important feature is the relative height of the atoms. According to Figure 4, Pt seems to be far from the surface (high-intensity profile), and Ag seems to be closer to the surface (lower-intensity profile). This apparent contradiction, with the previous structural analysis, is due to the intensity profile, which is highly dependent on the theoretical bias voltage used. For the systems studied above, we can point out that more states are excited inside the group 10 metals compared to the group 11 metals at 1.5 V. This behavior was previously described experimentally for the Au monomers, the Au + CO adsorbed on the NiAl surfaces,[51] and the Cu adsorbed on the Cu(111) surface.[9] However, it is possible to better understand this observation with more detailed descriptions of the electronic structure.

The projected density of states (PDOS) is a powerful tool used to elucidate how the electronic states of each species couple with each other. Figure 5 exhibits the density-of-states plots for all the studied systems. As a general rule, the plots represent the d states. The closest substrate surface atoms to the supported chain are depicted in black (Ni) and blue (Al); the main metal chain is represented by a red line and the dopant by a green line. The pristine LAC PDOS is in the diagonal plots.

From Figure 5, compared with the surface Ni (bold black line), the Al atom does not provide a major contribution in the "d" state PDOS (blue line). All the electronic interactions with the adatoms and the surface Al have "sp"-localized-type character (not shown here because of its low intensity). Carling et al. also observed this behavior for the Pt monomer adsorption on the NiAl(110) (here extended to other TMs of groups 10 and 11); on this occasion, because of the low "d" coupling ("sp" character), they stated that the metallic Al−adatom bonding might have a polar and a more ionic character.[30]

On the other hand, the Ni d states are very intense and show good coupling along the metal chain, which can be understood as a covalent metallic bond.[30] A major observation relies on the fact that, for the main LACs of the heavy metal group 11 (Ag and Au), the Ni PDOS exhibits a single band centered at >−2 eV; meanwhile, for the main LACs of group 10, the Ni PDOS

is highly broadened (and the most intense peak is shifted to energies below −2 eV). With an intermediate behavior, Cu causes Ni PDOS unfolding and is split into two bands: an intense one centered at ∼−2 eV and another centered at ∼−3 eV because of the high coupling of Ni and Cu d states. This behavior is not observed in any of the other analogous systems.

The electronic density of the states in group 11 has been widely reported for analogous[30,36,46,50] and different types of systems.[49,52,53] For instance, regarding Ag and Au as adsorbates, when the lateral interactions between the adsorbed atoms are negligible (e.g., in monomer cases),[35] one can observe a typical sharp and well-defined band centered at ∼−4 eV. Such a behavior is observed when Ag or Au acts as a dopant, indicating a very low coupling along the d states with group 10 metals. However, for the main Ag or Au LACs, that is, in the cases in which the lateral interactions play a major role, the d PDOS becomes clearly broader.[38,45]

For group 10 metals, Figure 5 shows that Pd and Pt have similar PDOS profiles. In fact, a careful look shows no significant changes in the shape of the electronic distribution, whether the metal is acting as either the main metal or the dopant. The Ni surface atoms and both Pd and Pt belong to the same group, showing an effective coupling.

The electron density difference matrix $\Delta\rho(xyz)$ (eq 4) is a well-established and useful tool[26,27,30] to further understand trends in formation of chemical bonds. In a similar approach to that used in eqs 1−3, 4 takes into account the difference in the electron density of the total system ($\Delta\rho_{tot}(xyz)$) with respect to the isolated surface ($\Delta\rho_{surf}(xyz)$) and the isolated chain ($\Delta\rho_{chain}(xyz)$).

$$\Delta\rho(xyz) = \rho_{tot}(xyz) - \rho_{surf}(xyz) - \rho_{chain}(xyz) \qquad (4)$$

A comparison of the LAC electron density difference plots can be seen in Figure 6 in which the pallet of colors varies from blue (charge depletion) to red (charge accumulation). More specifically, Figure 6 exhibits the cut along the chain plane in the [001] direction. In the Supporting Information, the structures from other angle views and directions are also shown (Figures S1−S5).

Regarding group 11 main LACs, two distinct behaviors are observed depending on the group to which the dopant belongs. First, when both the dopant and the main atom belong to group 11 (mixed LACs: $Ag_{main}-Au_{dop}$, $Ag_{main}-Cu_{dop}$, $Au_{main}-Ag_{dop}$, $Au_{main}-Cu_{dop}$, $Cu_{main}-Ag_{dop}$, and $Cu_{main}-Au_{dop}$), a very intense electron density accumulation (yellow to red) is observed between the surface and the chain as well as some electron density accumulation atop the chain atoms. Second, for group 10 dopants (LACs: $Ag_{main}-Pd_{dop}$, $Ag_{main}-$

Pt_{dop}, Au_{main}–Pd_{dop}, Au_{main}–Pt_{dop}, Cu_{main}–Pd_{dop}, and Cu_{main}–Pt_{dop}), the electron density accumulation between the surface and the chain is less intense (lying in the green region), but a very intense electron density accumulation is observed, noted by the small red area inside the dopant atom. These two observations imply that the electron density accumulation between the surface and the chain for the main atoms of group 11 is highly dependent on the dopant.

On the other hand, for group 10 LACs, no significant changes are observed concerning the electron density difference profile in the surface–chain interface (as seen in columns a and b in Figure 6) regardless of the chemical nature of the dopant. Furthermore, it is possible to identify an expressive electron density accumulation in the interatomic space along the chain, illustrated by the intense red domains inside the main atoms in the LAC. Here, it is worth mentioning that a deep difference in the charge density profile is observed for all Pt main LACs, depending on the distance between the Pt and the dopant (i.e., if the Pt is immediately close to or if it is far from the dopant). Such an observation leads us to conclude that the electronic structure of Pt is highly affected by the dopant.

Another analysis of the electron densities can be done by evaluating the atomic Bader charges. These charges were evaluated for every atom in all systems. First, the mean charge (in the electronic charge unit, e) of the pristine LAC system (q_{pris}) was found to be: Pd (0.644), Pt (0.933), Cu (0.202), Ag (0.167), and Au (0.502). Subsequently, for the mixed metal LACs, we chose to use the dopant atom charge (q_{dop}) as a probe and further observe how the charge is affected by the electronegativity of the main-chain atoms. The variation in the charge ($\Delta q = q_{dop} - q_{pris}$) of the dopant with respect to the main-chain composition is plotted in Figure 7a–e.
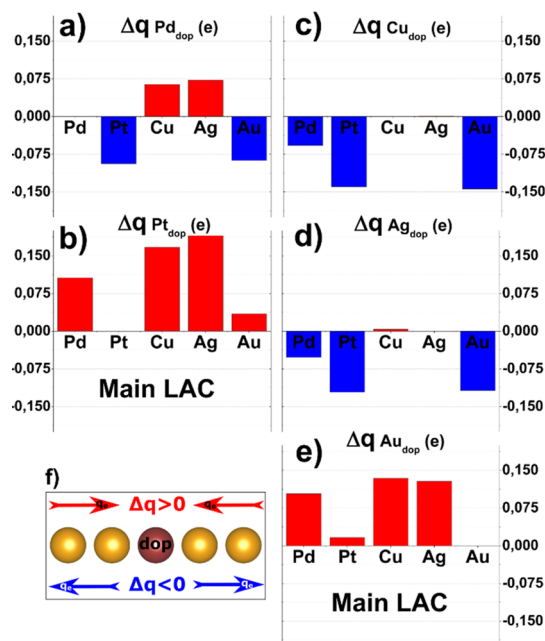

Figure 7. Positive values (red) indicate the dopant charge gain; negative values (blue) indicate the dopant charge loss; null values are expected for pristine LACs. (a–e) Mean Bader charge variation for the dopants with respect to the main LAC plots. (f) Simple chart of the electronegativity effect.

A careful look at Figure 7 shows some interesting properties concerning the electronegativity of the metals of groups 10 and 11. For example, as dopants, Pt and Au charges are always higher when compared with the pristine LAC; hence, for every main atom system, the Pt and Au LACs withdraw the electron density from the main chain. In other words, both Pt and Au exhibit higher electronegativity for the series.

On the other hand, Ag and Cu behave alike, in the sense that both have an analogous charge and always have a lower charge than that of the pristine LAC case, transferring the charge to the main LAC atoms. For Pd, there is an intermediate behavior; it loses the charge for the Au and Pt main atoms and gains the charge from the Ag and Cu main atoms. As a partial conclusion, it is possible to claim that Pt and Au are the most electronegative atoms, Ag and Cu are electropositive, and Pd is an intermediate case.

Besides the dopant mean charge, the individual atom charges in the chain are very meaningful. In particular, the main atoms are not equivalent in the chain, the dopant highly affects the density charge of the neighboring atoms, and consequently, the Bader charges may fluctuate along the atoms in the chain. This charge is significant because it explicitly exhibits the charge flux between the atoms. The Supporting Information (Tables S5–S9) shows the charge of the individual atoms in the chain for all the studied LAC systems. The main atoms with indexes 1 and 2 depict the far-away atoms, and the main atom indexes 3 and 4 are the dopant neighbors (Figure 1 shows the model used). A careful analysis of the tables in the Supporting Information suggests the following electronegativity trend: Pt > Au $\gg$ Pd $\gg$ Cu > Ag.

It is well established that adsorbates may deeply affect the surface electronic structure. In that sense, one property that is highly affected by the presence of an adsorbate is the work function (Φ). The work function is the amount of energy needed to drag one surface electron toward a vacuum. The absolute values of the work function are not commonly significant, but differences ($\Delta\Phi$) between the work function values for the systems before and after the adsorption processes are particularly meaningful.

In the DFT calculations, for the surface systems, the electrostatic potential along the z direction ($V(z)$) converges to a flat and well-defined value at the vacuum region. Our computational model is not symmetric: one surface contains the LAC atoms, whereas the other is clean. For each surface, there is a different converged electrostatic potential value, and the difference between them is indeed the work function change, $\Delta\Phi$, for the system.[54] Figure 8a exhibits the values of the work function changes for each system.

There is a traditional rule establishing a correlation between the work function changes and the electronic reorganization upon the adsorption process. Thus, if the adsorbate withdraws the electron density from the substrate, there will be an increase in the work function. In contrast, when the adsorbate donates the electron density to the surface, a decrease in the work function is expected.

However, for several systems, this general rule sometimes fails on predictions,[55,56] and a more detailed description is needed. It is necessary to understand how the surface electron density distribution may affect the work function. As a matter of fact, for the atoms of groups 10 and 11 adsorbed on the NiAl(110) surface, the electronegativity is not sufficient to fully understand the trends in the work function changes, as already reported in previous publications.[35,38] Similar discussions on
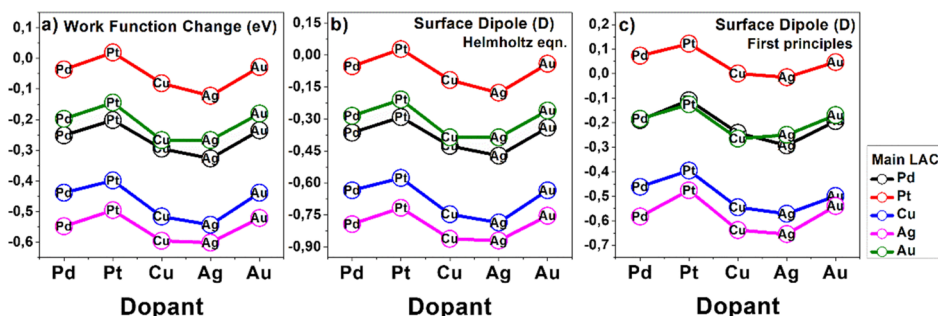
Figure 8. Work function and surface dipole models. (a) Work function changes (in eV). (b) Surface dipole (in D) using the Helmholtz model (eq 5). (c) Surface dipole obtained from first-principle calculations (eq S3). The main-chain atoms are indicated by the colored lines, and the dopants are indicated by the circles.

the modified local surface dipole of the metal surfaces by different effects such as molecular adsorption or ionic layer covering have been reported.[57]

A known elegant description[55,56,58−60] quantitatively connects the dipole moment change ($\Delta\mu$) (or simply the surface dipole) with the electron density difference (eq 4) of the system. The planar averaged electron density ($\Delta\rho(z)$) is obtained by averaging in the (x,y) plane, and the dipole moment density is scaled along the z direction ($\Delta\rho(z)\cdot z$). These two curves are plotted for pristine LACs in Figure 9, and
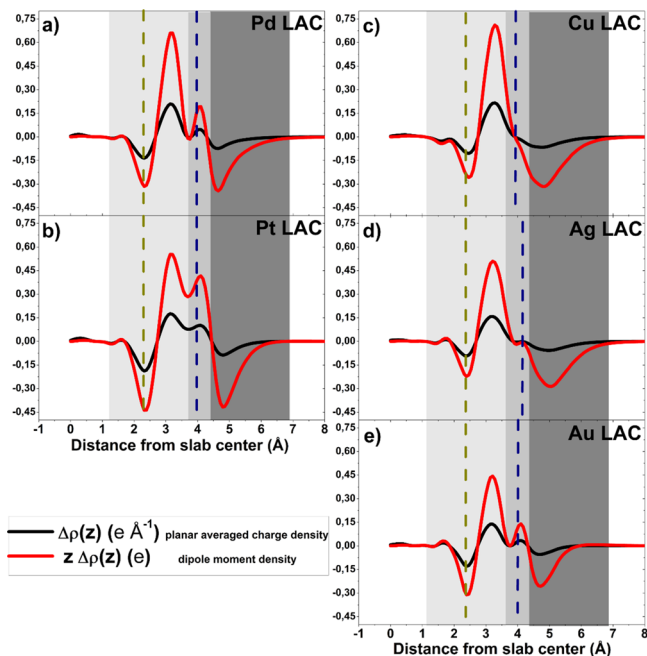

Figure 9. (a−e) Planar averaged charge density $\Delta\rho(z)$ (e Å^{-1}) in the black line and the dipole moment density ($\Delta\rho(z)\cdot z$) (e) in the red. Vertical dashed lines indicate the top surface Ni and the main metal atom positions.

they can provide critical information about the electron-charge transfer in the adsorbate−substrate. The resulting surface dipole is the integration in the **z** direction. More details of the method are provided in the Supporting Information.

Three relevant ranges are highlighted in Figure 9. The first (in light gray) is the space between the NiAl surface and the chain (∼1.7 Å to 3.7 Å). A valley followed by a peak can be observed. Physically, this represents the withdrawn electron density from the NiAl surface toward the chain structure,

which is the effect of the atom electronegativity. Group 10 atoms (Pd and Pt) exhibit the most prominent depletion zones.

The medium gray area (∼3.7 Å to 4.6 Å) corresponds to a secondary electronegativity effect. It relates to the electron density accumulation in the LAC atoms; in these cases, the less-electronegative atoms exhibit very modest peaks (even not observable for Cu).

The third zone (in dark gray) can be understood as the electron density reorganization above the atomic chain and is therefore related to the polarizability. As a matter of fact, this is an important zone regarding the values of $\Delta\mu$. According to eq S2, the further away from the slab center, the higher the effects on $n(z)$ will be and, consequently, the greater the effects on the $\Delta\mu$ will be (eq S3). For instance, Ag and Cu (the most polarizable atoms) display the most intense valleys; therefore, the integration of this area (negative values) pushes the surface dipole moment to lower values (as can be observed in Figure 9c).

For a comparison, the surface dipole was also obtained using the Helmholtz model[61] (eq 5), where the surface dipole $\Delta\mu$ is linearly connected with the surface working function change $\Delta\Phi$ and the computational model parameter A (slab surface area) and Θ (surface coverage), scaled by the constants e (elementary charge) and ε_0 (vacuum permittivity).[a] The values of the dipole moment differences were obtained for all the mixed-metal LAC systems. In Figure 8b,c, the graph exhibits trends in the values for $\Delta\mu$ (lines) as a function of the dopant for both the Helmholtz model and the first-principle calculations approach, respectively. The same trends and the linear relation with the work function differences are observed from Figure 8a.

$$\Delta\mu = \frac{e}{\varepsilon_0}\frac{\Delta\Phi A}{\Theta} \tag{5}$$

From Figure 8a, all the work function changes induced by the presence of the pristine LACs are negative values (except for pristine Pt LAC), which would not be expected from the traditional arguments considering that all TMs are more electronegative than the support. Furthermore, the surface dipole values shown in Figure 8c are larger than those obtained from the Helmholtz equation (Figure 8b). A more detailed analysis shows that these differences are about 0.2 D for the metals with low-electronegativity and high-polarizability atoms (Ag and Cu) and about 0.1 D for high-electronegativity and low-polarizability atoms (Au and Pt).

Deviances from purely electrostatic models (i.e., the Helmholtz equation) would be more significant when dealing with more polarizable systems, as was observed in Figure 9. Thus, the alloying of pristine LACs constitutes a way to model systems with controlled local dipoles and consequently, with the desired work function changes.

CONCLUSIONS

In this study, we have explored the electronic and structural properties of TM chains (one-atom-thick), namely, LACs, and the effects when alloying with other metals of groups 10 and 11. Although the first LACs were built using STM techniques in the earlier 2000s, there has not been much progress since then. Here, we report the first comparative study using DFT calculations, intending to rationalize the physical−chemical properties of these systems to model nanodevices with specific functionalities to be used in different technological areas, such as molecular adsorption, catalysis, and transport properties.

Metal dopants modify the electron density distribution of the pristine LACs, creating regions with charge depletion (using Cu and Ag dopants) or charge accumulation (using Pt and Au dopants), and this effect might be used to trap small molecules selectively conducting to specific pathways in chemical reactions or also enhancing spectroscopic properties. It was possible to establish the following electronegativity series: (Pt > Au > Pd > Cu > Ag).

Therefore, using computational modeling, which has now reached a high degree of predictive potential, we presented these new systems, namely, alloy LACs, which nowadays can be experimentally built, and showed interesting results that can be helpful in the area of nanoscience.

METHODOLOGY

All results presented in this work were based on the DFT calculations using the Vienna Ab initio Simulation Package. The plane waves basis set[62,63] was set up with the kinetic energy cutoff set to 300 eV (to obtain converged energies below 1 meV/atom). Plane waves were used to describe the valence electrons, and the inner electrons were treated using the projector-augmented wave method.[64,65]

The Brillouin zone was sampled with a 2 × 3 × 1 Monkhorst−Pack grid[66] for structural optimization, and with a 4 × 6 × 1 grid for single-point electronic optimization, using the Methfessel−Paxton[67] method with a smearing width of 0.1 eV. The conjugated-gradient[68] algorithm was used for structural ionic optimization with the Hellmann−Feynman forces converged to a less than 0.005 eV/Å atom. The generalized gradient approximation with the Perdew−Wang[69] (PW91) functional was used for the exchange/correlation energy contribution. All the calculations were spin-polarized.

The HIVE-STM software[70] uses the Tersoff−Hamann[71] methodology to simulate STM images and further qualitatively discuss the electronic states' coupling at the surface. The atomic Bader charges were evaluated using Henkelman's group algorithms.[72−74] The Bader analysis is a well-established tool to provide a quantitative description of the atomic charges and further evaluate the quantitative description of the electronegativity of the atoms.

The surface area of this model is quite large to attenuate the periodic boundary conditions bias (and have a more realistic support). All the results were obtained for the substrate by an asymmetric slab approach (i.e., the adsorbed atoms were deposited at only one slab side).

ASSOCIATED CONTENT

ⓢ Supporting Information

The Supporting Information is available free of charge on the ACS Publications website at DOI: 10.1021/acsomega.8b00817.

> Structural analyses values of the charge difference isosurfaces for all the systems studied along the various perspectives and cell cuts; comparison of the Bader charge obtained individually for all the atoms in the chains; and more details of the dipole moment model (PDF)

AUTHOR INFORMATION

Corresponding Author

*E-mail: smiguel@iqm.unicamp.br. Phone: +55 (19) 3521-3441 (M.A.S-M.).

ORCID Ⓘ

Edison Zacarias da Silva: 0000-0002-2195-0051
Miguel Angel San-Miguel: 0000-0002-6650-7432

Notes

The authors declare no competing financial interest.

ACKNOWLEDGMENTS

ADDITIONAL NOTE

[a]A note concerning the Helmholtz equation may be useful: the equation used by Li et al. (*Phys. Rev. B: Condens. Matter Mater. Phys.* **2002**, *65* (7), 075407), usually omits the term e/ε_0; numerically, the results make sense (in D), but the dimensions of both terms in the equation do not agree. Here, we chose the most complete form of the Helmholtz equation.

REFERENCES

(1) Eigler, D. M.; Schweizer, E. K. Positioning Single Atoms with a Scanning Tunnelling Microscope. *Nature* **1990**, *344*, 524−526.
(2) Stroscio, J. A.; Eigler, D. M. Atomic and Molecular Manipulation with the Scanning Tunneling Microscope. *Science* **1991**, *254*, 1319−1326.
(3) Rubio-Bollinger, G.; Bahn, S. R.; Agraït, N.; Jacobsen, K. W.; Vieira, S. Mechanical Properties and Formation Mechanisms of a Wire of Single Gold Atoms. *Phys. Rev. Lett.* **2001**, *87*, 026101.
(4) da Silva, E.; da Silva, A.; Fazzio, A. How Do Gold Nanowires Break? *Phys. Rev. Lett.* **2001**, *87*, 256102.
(5) Ohnishi, H.; Kondo, Y.; Takayanagi, K. Quantized Conductance through Individual Rows of Suspended Gold Atoms. *Nature* **1998**, *395*, 780−783.
(6) Nitzan, A.; Ratner, M. A. Electron Transport in Molecular Wire Junctions. *Science* **2003**, *300*, 1384−1389.

(7) Joachim, C.; Gimzewski, J. K.; Aviram, A. Electronics Using Hybrid-Molecular and Mono-Molecular Devices. *Nature* **2000**, *408*, 541−548.

(8) Cretu, O.; Botello-Mendez, A. R.; Janowska, I.; Pham-Huu, C.; Charlier, J.-C.; Banhart, F. Electrical Transport Measured in Atomic Carbon Chains. *Nano Lett.* **2013**, *13*, 3487−3493.

(9) Díaz-tendero, S.; Fölsch, S.; Olsson, F. E.; Borisov, A. G.; Gauyacq, J.-P. Electron Propagation along Cu Atomic Wires Supported on a Cu (111) Surface. *Nano Lett.* **2008**, *8*, 2712−2717.

(10) Díaz-tendero, S.; Olsson, F. E.; Borisov, A. G.; Gauyacq, J.-P. Excited Electron Dynamics in Cu Nanowires Supported on a Cu(111) Surface. *Phys. Rev. B: Condens. Matter Mater. Phys.* **2009**, *79*, 115438.

(11) Díaz-Tendero, S.; Borisov, A. G.; Gauyacq, J.-P. Extraordinary Electron Propagation Length in a Metallic Double Chain Supported on a Metal Surface. *Phys. Rev. Lett.* **2009**, *102*, 166807.

(12) Rodrigues, V.; Ugarte, D. Real-Time Imaging of Atomistic Process in One-Atom-Thick Metal Junctions. *Phys. Rev. B: Condens. Matter Mater. Phys.* **2001**, *63*, 073405.

(13) Nascimento, A. P. F.; San-Miguel, M. A.; Da Silva, E. Z. Unveiling the Origin of Oxygen Atomic Impurities in Au Nanowires. *Phys. Rev. B: Condens. Matter Mater. Phys.* **2014**, *89*, 085417.

(14) Zhang, K.; Hu, X.; Liu, J.; Yin, J.-J.; Hou, S.; Wen, T.; He, W.; Ji, Y.; Guo, Y.; Wang, Q.; et al. Formation of PdPt Alloy Nanodots on Gold Nanorods: Tuning Oxidase-like Activities via Composition. *Langmuir* **2011**, *27*, 2796−2803.

(15) He, W.; Wu, X.; Liu, J.; Zhang, K.; Chu, W.; Feng, L.; Hu, X.; Zhou, W.; Xie, S. Pt-Guided Formation of Pt−Ag Alloy Nanoislands on Au Nanorods and Improved Methanol Electro-Oxidation. *J. Phys. Chem. C* **2009**, *113*, 10505−10510.

(16) Chen, W.; Yu, R.; Li, L.; Wang, A.; Peng, Q.; Li, Y. A Seed-Based Diffusion Route to Monodisperse Intermetallic CuAu Nano-crystals. *Angew. Chem., Int. Ed.* **2010**, *49*, 2917−2921.

(17) Yin, A.; Wen, C.; Dai, W.-L.; Fan, K. Nanocasting of CuAu Alloy Nanoparticles for Methyl Glycolate Synthesis. *J. Mater. Chem.* **2011**, *21*, 8997−8999.

(18) Ferrando, R.; Jellinek, J.; Johnston, R. L. Nanoalloys: From Theory to Applications of Alloy Clusters and Nanoparticles. *Chem. Rev.* **2008**, *108*, 845−910.

(19) Pittaway, F.; Paz-Borbón, L. O.; Johnston, R. L.; Arslan, H.; Ferrando, R.; Mottet, C.; Barcaro, G.; Fortunelli, A. Theoretical Studies of Palladium−Gold Nanoclusters: Pd−Au Clusters with up to 50 Atoms. *J. Phys. Chem. C* **2009**, *113*, 9141−9152.

(20) Bouderbala, W.; Boudjahem, A.-G.; Soltani, A. Geometries, stabilities, electronic and magnetic properties of small PdnIr (n= 1-8) clusters from first-principles calculations. *Mol. Phys.* **2014**, *112*, 1789−1798.

(21) Datta, S.; Raychaudhuri, A. K.; Saha-Dasgupta, T. First principles study of bimetallic Ni13−nAgn nano-clusters (n = 0-13): Structural, mixing, electronic, and magnetic properties. *J. Chem. Phys.* **2017**, *146*, 164301.

(22) Yan, J.; Gao, S. Plasmon Resonances in Linear Atomic Chains: Free-Electron Behavior and Anisotropic Screening of D Electrons. *Phys. Rev. B: Condens. Matter Mater. Phys.* **2008**, *78*, 235413.

(23) Fan, M.; Lai, F.-J.; Chou, H.-L.; Lu, W.-T.; Hwang, B.-J.; Brolo, A. G. Surface-Enhanced Raman Scattering (SERS) from Au:Ag Bimetallic Nanoparticles: The Effect of the Molecular Probe. *Chem. Sci.* **2013**, *4*, 509−515.

(24) Xie, W.; Herrmann, C.; Kömpe, K.; Haase, M.; Schlücker, S. Synthesis of Bifunctional Au/Pt/Au Core/shell Nanoraspberries for in Situ SERS Monitoring of Platinum-Catalyzed Reactions. *J. Am. Chem. Soc.* **2011**, *133*, 19302−19305.

(25) Mayer, K. M.; Hafner, J. H. Localized Surface Plasmon Resonance Sensors. *Chem. Rev.* **2011**, *111*, 3828−3857.

(26) Davis, H. L.; Noonan, J. R. Rippled Relaxation in the (110) Surface of the Ordered Metallic Alloy NiAl. *Phys. Rev. Lett.* **1985**, *54*, 566−569.

(27) Kang, M. H.; Mele, E. J. NiAl(110) surface: First-principles determination of the rippled relaxation. *Phys. Rev. B: Condens. Matter Mater. Phys.* **1987**, *36*, 7371−7377.

(28) Lee, J. I.; Fu, C. L.; Freeman, A. J. All-electron local-density theory of the rippled NiAl(110) surface. *Phys. Rev. B: Condens. Matter Mater. Phys.* **1987**, *36*, 9318−9321.

(29) Kogita, T.; Kohyama, M.; Kido, Y. Structure and Dynamics of NiAl(110) Studied by High-Resolution Ion Scattering Combined with Density Functional Calculations. *Phys. Rev. B: Condens. Matter Mater. Phys.* **2009**, *80*, 235414.

(30) Carling, K. M.; Glover, W.; Gunaydin, H.; Mitchell, T. A.; Carter, E. A. Comparison of S, Pt, and Hf adsorption on NiAl(110). *Surf. Sci.* **2006**, *600*, 2079−2090.

(31) Hanbicki, A. T.; Baddorf, A. P.; Plummer, E. W.; Hammer, B.; Scheffler, M. The interaction of hydrogen with the (110) surface of NiAl. *Surf. Sci.* **1995**, *331−333*, 811−817.

(32) Evecen, M.; Çakmak, M. Adsorption of S, O, and H on the NiAl(110)-(2×2) surface. *Phys. B Condens. Matter* **2010**, *405*, 4059−4063.

(33) Borck, Ø.; Svenum, I.-H.; Borg, A. Adsorption of Methanol and Methoxy on NiAl(110) and Ni3Al(111): A DFT Study. *Surf. Sci.* **2009**, *603*, 2378−2386.

(34) Svenum, I.-H.; Borck, Ø.; Schulte, K.; Walle, L. E.; Borg, A. Adsorption of Methanol on Ni3Al(111) and NiAl(110): A High Resolution PES Study. *Surf. Sci.* **2009**, *603*, 2370−2377.

(35) San-Miguel, M. A.; Amorim, E. P. M.; da Silva, E. Z. Adsorption of Pd, Pt, Cu, Ag, and Au Monomers on NiAl(110) Surface: A Comparative Study from DFT Calculations. *J. Phys. Chem. A* **2013**, *118*, 5748−5755.

(36) Calzolari, A.; Buongiorno Nardelli, M. First Principles Theory of Artificial Metal Chains on NiAl(110) Surface. *Phys. Rev. B: Condens. Matter Mater. Phys.* **2005**, *72*, 045416.

(37) Persson, M. Computational Study of Electron States in Au Chains on NiAl(110). *Phys. Rev. B: Condens. Matter Mater. Phys.* **2004**, *70*, 205420.

(38) San-Miguel, M. A.; Amorim, E. P. M.; da Silva, E. Z. NiAl(110) Surface as a Template for Growing Transition Metal Linear Atomic Chains: A DFT Investigation. *J. Phys. Chem. C* **2015**, *119*, 2456−2461.

(39) Nilius, N.; Wallis, T. M.; Ho, W. Development of One-Dimensional Band Structure in Artificial Gold Chains. *Science* **2002**, *297*, 1853−1856.

(40) Wallis, T. M.; Nilius, N.; Ho, W. Electronic Density Oscillations in Gold Atomic Chains Assembled Atom by Atom. *Phys. Rev. Lett.* **2002**, *89*, 236802.

(41) Nilius, N.; Wallis, T. M.; Persson, M.; Ho, W. Distance Dependence of the Interaction between Single Atoms: Gold Dimers on NiAl(110). *Phys. Rev. Lett.* **2003**, *90*, 196103.

(42) Nilius, N.; Wallis, T. M.; Ho, W. Building Alloys from Single Atoms: Au−Pd Chains on NiAl(110)†. *J. Phys. Chem. B* **2004**, *108*, 14616−14619.

(43) Nilius, N.; Wallis, T. M.; Ho, W. Realization of a Particle-in-a-Box: Electron in an Atomic Pd Chain. *J. Phys. Chem. B* **2005**, *109*, 20657−20660.

(44) Taylor, A.; Doyle, N. J. Further studies on the nickel-aluminium system. I. β-NiAl and δ-Ni2Al3phase fields. *J. Appl. Crystallogr.* **1972**, *5*, 201−209.

(45) Zornio, B. F.; da Silva, E. Z.; San-Miguel, M. A. Exploring from Ab Initio Calculations the Structural and Electronic Properties of Supported Metal Linear Atomic Chains on the NiAl (110) Surface. *Theor. Chem. Acc.* **2017**, *136*, 62.

(46) Wu, P.; Yin, N.; Cheng, W.; Li, P.; Huang, M. Structure and electronic properties of palladium chains supported by NiAl(1 1 0): A first-principles study. *Comput. Mater. Sci.* **2016**, *124*, 398−402.

(47) Callister, W. D., Jr. *Material Science and Engineering*, 6th ed.; John Wiley & Sons: Danvers, MA, 2003.

(48) Kiejna, A. Comparative Study of Ag, Au, Pd, and Pt Adsorption on Mo and Ta (112) Surfaces. *Phys. Rev. B: Condens. Matter Mater. Phys.* **2006**, *74*, 235429.

(49) Zarechnaya, E. Y.; Skorodumova, N. V.; Simak, S. I.; Johansson, B.; Isaev, E. I. Theoretical Study of Linear Monoatomic Nanowires, Dimer and Bulk of Cu, Ag, Au, Ni, Pd and Pt. *Comput. Mater. Sci.* **2008**, *43*, 522−530.

(50) Wu, P.; Cao, G.; Tang, F.; Huang, M. First-principles study of small palladium clusters on NiAl(110) alloy surface. *Phys. E* **2013**, *53*, 7−13.

(51) Wallis, T. M.; Nilius, N.; Ho, W. Single Molecule Vibrational and Electronic Analyses of the Formation of Inorganic Complexes: CO Bonding to Au and Ag Atoms on NiAl(110). *J. Chem. Phys.* **2003**, *119*, 2296−2300.

(52) Giordano, L.; Baistrocchi, M.; Pacchioni, G. Bonding of Pd, Ag, and Au Atoms on MgO(100) Surfaces and MgO/Mo(100) Ultra-Thin Films: A Comparative DFT Study. *Phys. Rev. B: Condens. Matter Mater. Phys.* **2005**, *72*, 115403.

(53) Hernández, N. C.; Graciani, J.; Márquez, A.; Sanz, J. F. Cu, Ag and Au atoms deposited on the α-Al2O3(0001) surface: a comparative density functional study. *Surf. Sci.* **2005**, *575*, 189−196.

(54) Kiejna, A. Work Function of Metals. In *Reference Module in Chemistry, Molecular Sciences and Chemical Engineering*; Reedijk, J., Ed.; Elsevier Inc.: Waltham, MA, 2014; pp 1−8.

(55) Michaelides, A.; Hu, P.; Lee, M.-H.; Alavi, A.; King, D. A. Resolution of an Ancient Surface Science Anomaly: Work Function Change Induced by N Adsorption on W{100}. *Phys. Rev. Lett.* **2003**, *90*, 246103.

(56) Leung, T. C.; Kao, C. L.; Su, W. S.; Feng, Y. J.; Chan, C. T. Relationship between Surface Dipole, Work Function and Charge Transfer: Some Exceptions to an Established Rule. *Phys. Rev. B: Condens. Matter Mater. Phys.* **2003**, *68*, 195408.

(57) Robledo, M.; Pacchioni, G.; Martín, F.; Alcamí, M.; Díaz-Tendero, S. Adsorption of Benzene on Cu(100) and on Cu(100) Covered with an Ultrathin NaCl Film: Molecule-Substrate Interaction and Decoupling. *J. Phys. Chem. C* **2015**, *119*, 4062−4071.

(58) Rusu, P. C.; Brocks, G. Surface Dipoles and Work Functions of Alkylthiolates and Fluorinated Alkylthiolates on Au(111). *J. Phys. Chem. B* **2006**, *110*, 22628−22634.

(59) Zeng, Z.-H.; Da Silva, J. L. F.; Li, W.-X. Theory of nitride oxide adsorption on transition metal (111) surfaces: a first-principles investigation. *Phys. Chem. Chem. Phys.* **2010**, *12*, 2459−2470.

(60) Arefi, H. H.; Fagas, G. Chemical Trends in the Work Function of Modified Si(111) Surfaces: A DFT Study. *J. Phys. Chem. C* **2014**, *118*, 14346−14354.

(61) Li, W.-X.; Stampfl, C.; Scheffler, M. Oxygen Adsorption on Ag(111): A Density-Functional Theory Investigation. *Phys. Rev. B: Condens. Matter Mater. Phys.* **2002**, *65*, 075407.

(62) Kresse, G.; Furthmüller, J. Efficiency of Ab-Initio Total Energy Calculations for Metals and Semiconductors Using a Plane-Wave Basis Set. *Comput. Mater. Sci.* **1996**, *6*, 15−50.

(63) Kresse, G.; Furthmüller, J. Efficient iterative schemes forab initiototal-energy calculations using a plane-wave basis set. *Phys. Rev. B: Condens. Matter Mater. Phys.* **1996**, *54*, 11169−11186.

(64) Blöchl, P. E. Projector Augmented-Wave Method. *Phys. Rev. B: Condens. Matter Mater. Phys.* **1994**, *50*, 17953−17979.

(65) Kresse, G.; Joubert, D. From Ultrasoft Pseudopotentials to the Projector Augmented-Wave Method. *Phys. Rev. B: Condens. Matter Mater. Phys.* **1999**, *59*, 1758−1775.

(66) Monkhorst, H. J.; Pack, J. D. Special Points for Brillouin-Zone Integrations. *Phys. Rev. B: Solid State* **1976**, *13*, 5188−5192.

(67) Methfessel, M.; Paxton, A. T. High-Precision Sampling for Brillouin-Zone Integration in Metals. *Phys. Rev. B: Condens. Matter Mater. Phys.* **1989**, *40*, 3616−3621.

(68) Payne, M. C.; Teter, M. P.; Allan, D. C.; Arias, T. A.; Joannopoulos, J. D. Iterative minimization techniques forab initiototal-energy calculations: molecular dynamics and conjugate gradients. *Rev. Mod. Phys.* **1992**, *64*, 1045−1097.

(69) Perdew, J. P.; Chevary, J. A.; Vosko, S. H.; Jackson, K. A.; Pederson, M. R.; Singh, D. J.; Fiolhais, C. Atoms, Molecules, Solids, and Surfaces: Applications of the Generalized Gradient Approx-imation for Exchange and Correlation. *Phys. Rev. B: Condens. Matter Mater. Phys.* **1992**, *46*, 6671−6687.

(70) Vanpoucke, D. E. P.; Brocks, G. Formation of Pt-Induced Ge Atomic Nanowires on Pt/Ge (001): A Density Functional Theory Study. *Phys. Rev. B: Condens. Matter Mater. Phys.* **2008**, *77*, 241308.

(71) Tersoff, J.; Hamann, D. R. Theory and Application for the Scanning Tunneling Microscope. *Phys. Rev. Lett.* **1983**, *50*, 1998−2001.

(72) Henkelman, G.; Arnaldsson, A.; Jónsson, H. A Fast and Robust Algorithm for Bader Decomposition of Charge Density. *Comput. Mater. Sci.* **2006**, *36*, 354−360.

(73) Tang, W.; Sanville, E.; Henkelman, G. A Grid-Based Bader Analysis Algorithm without Lattice Bias. *J. Phys. Condens. Matter* **2009**, *21*, 084204.

(74) Sanville, E.; Kenny, S. D.; Smith, R.; Henkelman, G. Improved Grid-Based Algorithm for Bader Charge Allocation. *J. Comput. Chem.* **2007**, *28*, 899−908.